Two-Layer Optimization Framework for the Sizing and Operation of Hydrogen-Integrated Multi-Energy Systems

Lorenzo Gasperin[a], Simone Peccolo[a], Francesco Nascimben[a], Anna Stoppato[a] and Alberto Benato[b]

[a] *University of Padova, Padua, Italy,*
[b] *University of Padova, Padua, Italy, alberto.benato@unipd.it CA*

Abstract:
The integration of hydrogen subsystems into Multi-Energy Systems is becoming always more critical for industrial decarbonization. However, jointly optimizing capacity sizing and long-term operational dispatch remains computationally prohibitive when accounting for the physical degradation of components over time. Standard Mixed-Integer Linear Programming approaches become intractable when non-linear, time-dependent efficiency curves are introduced. To overcome this limitation, this study proposes a novel degradation-aware bi-level optimization framework. An outer Genetic Algorithm determines the optimal discrete sizing of the MES components, while an inner solver evaluates the cost-optimal 8760-hour operational dispatch. Crucially, the framework externalizes size-dependent performance parameters and employs a sequential heuristic-simulation approach over a 15-year project horizon. This allows the model to dynamically downgrade the piecewise-linearized efficiency curves of the electrolyser and fuel cells based on empirical voltage decay rates. Applied to a zero-emission industrial MES case study, the optimization prioritized maximized photovoltaic capacity and an oversized electrolyser, achieving a €16.9 million Net Present Cost reduction compared to a fossil-fuelled baseline. Furthermore, the sequential multi-year simulation revealed that unmitigated capacity fade severely alters the optimal dispatch; as the fuel cell degrades, the system is forced to increase external grid imports, driving a compounded 6% increase in Operational Expenditures. Ultimately, this framework provides a highly scalable tool to prevent the systemic underestimation of long-term costs in zero-emission energy infrastructures. .

Keywords:
Hydrogen-integrated multi-energy systems, Genetic Algorithm, Mixed Integer Linear Programming, technoeconomic optimisation,, Long-term operational optimization.

1. Introduction

The global decarbonization effort is driving an unprecedented deployment of Renewable Energy Sources (RES). However, the growing penetration of intermittent technologies, such as solar and wind, has exacerbated the temporal mismatch between non-dispatchable generation and user demand, necessitating robust energy storage and flexibility solutions [1], [2]. In this context, hydrogen has emerged as a critical green energy carrier, uniquely suited for long-term storage and multi-sectoral energy coupling [3], [4]. Integrating hydrogen subsystems, specifically Proton Exchange Membrane (PEM) electrolysers and fuel cells, into hybrid Multi-Energy Systems (MES) can effectively buffer these energy fluxes. However, the techno-economic performance of these devices is highly sensitive to part-load operation, conversion inefficiencies, and, critically, long-term physical degradation. While the scientific literature has extensively investigated the baseline modelling of hydrogen technologies [5], [6] capturing their long-term degradation remains a complex challenge. Extensive component level research has characterized PEM degradation mechanisms under both constant and dynamic

loads. For fuel cells, studies have successfully identified distinct stages of membrane decomposition [7], and quantified voltage decay under dynamic operations [8], [9]. Similar component-level degradation analyses have been conducted for PEM electrolysers [10], integrating these physics-based decay models into localized energy management strategies [11]. Parallel to component-level research, system-level design optimization has seen significant advancements. Metaheuristic algorithms, particularly Particle Swarm Optimization (PSO) and Genetic Algorithms (GA), are frequently coupled with Mixed-Integer Linear Programming (MILP) to resolve the complex, high-dimensional dispatch of hybrid microgrids [12]. These frameworks successfully balance conflicting objectives such as total system cost, emissions, and reliability. Despite these parallel advancements, a critical methodological gap persists: there is a distinct lack of comprehensive frameworks that bridge the physical reality of long-term component degradation with the high-resolution, system-level optimization of hybrid multi-energy networks. Existing approaches generally assess sizing over long-term horizons assuming constant efficiencies, or optimize hourly dispatch without penalizing the capacity fade and voltage decay accumulated over years of operation. To address this gap, this study proposes a novel, degradation-aware bi-level optimization framework. Combining an outer Genetic Algorithm (GA) with an inner Mixed-Integer Linear Programming (MILP) solver, the model simultaneously optimizes the capacity sizing and the hourly energy dispatch of an integrated hydrogen-based MES. Unlike traditional static models, this framework explicitly integrates multi-year membrane degradation trajectories for both the electrolyser and the fuel cell. Applied to an industrial neighbourhood case study in Italy, comprising PV generation, battery and thermal storage and grid interactions, this methodology quantifies how operational ageing dynamically alters system efficiency, dispatch schedules, and overall techno-economic viability across the project's lifetime.

2. Methods

2.1. Energy system model

From the perspective of the external electrical grid, the integrated multi-energy system is modelled as a single aggregated node. The use of storage devices facilitates the management of the stochastic fluctuations of RES and protects the external grid from direct intermittency effects. The interconnection with the external grid is bidirectional, enabling both the export of surplus generation and the opportunistic import of electricity to exploit hourly price arbitrage. Conversely, the interconnection with the end-users is strictly unidirectional, from the MES or the grid to the demand nodes. The structure of the MES, as reported in Figure 1, comprises a photovoltaic plant, a battery storage system, thermal energy storage, an industrial water boiler and an hydrogen subsystem. The hydrogen subsystem is specifically composed of a PEM electrolyser stacks, pressurized hydrogen storage vessels, and fuel cell stacks. Electrical generation assets (PVs and FCs) are constrained by three potential output streams: direct supply to the electrical demand node, charging fluxes to the EBs or electrical supply to the electrolysers for hydrogen production. Similarly, thermal generation assets (FCs and the boiler) are modelled with dual output streams: direct satisfaction of the user thermal load and charging fluxes to the TS. The integration of TS decouples thermal energy production from instantaneous user demand, mitigating "heat-driven" cogenerative operation. Finally, the EB and hydrogen storage units provide bidirectional flexibility, discharging to meet external user loads or supplying internal MES conversion processes. The core of the modelled MES relies on the mathematical representation of the hydrogen subsystem components. Proton exchange membrane technology was selected due to its low operating temperature, rapid start-up and shut-down cycling capabilities, and high flexibility in part-load management. These characteristics make PEM systems well-suited for direct integration with the highly intermittent power profiles of renewable energy sources [13]. A fundamental for the formulation was the development of a simple model that maintained the linearity required by the MILP solver, yet precise enough to capture real thermodynamic behaviour of the components. Furthermore, the mathematical model had to be scalable, remaining valid independent of the spe-

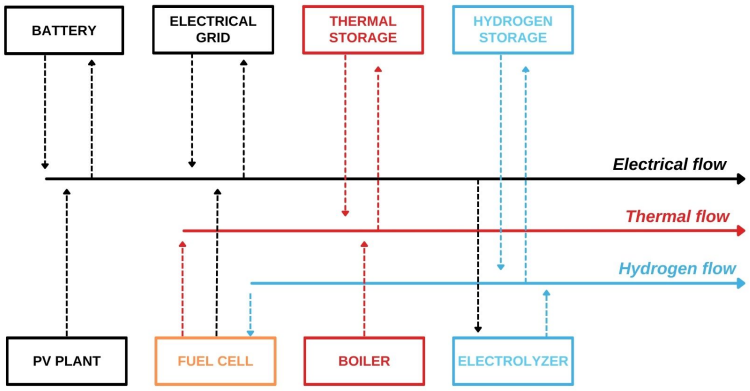

Figure 1: Simplified structure of the multi energy system.

cific number of stacks configured in series or parallel. To achieve this, an energy-based efficiency was computed. Building upon the model presented by [14], the PEM electrolyser efficiency was piecewise linearized to conform to the MILP constraints. The resulting linearized curve, reported in Figure 2, has been benchmarked against empirical literature and commercial performance data. The electrolyser formulation was cross validated against commercial polarization curves [15]. Sensitivity analyses, conducted across broad operating pressures (1 to 40 bar) and temperatures (50 to 90 °C), were performed to assure compliance under different operational conditions [16]. Across the operative range, the relative error remains constrained within a ±5% margin. The maximum relative deviation is isolated entirely to extreme low-load conditions (below 15% nominal capacity), where the error peaks transiently at approximately 13%. Similarly, the fuel cell performance curves were validated against multiple empirical models, including those by [17]. Evaluating the piecewise linear approximation under varying temperatures and pressures reveals a robust fit; the error stabilizes within a ±5% boundary for most of the normalized power input spectrum. The maximum observed deviation is strictly confined to approximately 8% at the lowest operational limits. These constrained error margins confirm that the selected efficiency curves induce negligible thermodynamic distortion, thereby validating their use within the optimization solver's linear constraints. Consequently, the operational output of the EL is evaluated directly in terms of energy, governed by Equation 1.

$$E_{out,EL} = E_{in,EL} * \eta_{EL} \tag{1}$$

Where $E_{out,EL}$ is the energy equivalent of the produced hydrogen, $E_{in,EL}$ is the electrical energy input and η_{EL} represents the piecewise-linearized conversion efficiency. Following a similar methodology of the EL, the electrical efficiency of the fuel cell was modelled using data derived from the same literature baseline [14]. The FCs are configured for CHP operation and the thermal efficiency of the FC subsystem was derived directly from the overall First Law efficiency. The governing equations for the FC energy output are defined in Equations 2, 3 and 4.

$$E_{out,FC} = E_{in,FC} * \eta_{el,FC} \tag{2}$$

$$\eta_{th,FC} = \eta_{tot,FC} - \eta_{el,FC} \tag{3}$$

$$Q_{out,FC} = E_{in,FC} * \eta_{th,FC} \tag{4}$$

where $E_{out,FC}$ is the electrical energy produced, $E_{in,FC}$ is the chemical energy of the hydrogen consumed, $\eta_{el,FC}$ and $\eta_{th,FC}$ are the respective electrical and thermal efficiencies, while $\eta_{tot,FC}$ is the overall efficiency. $Q_{out,FC}$ represents the recoverable thermal energy routed to the MES thermal network. The hydrogen storage system is modelled as a pressurized vessel directly connected to the

PEM Electrolyser. To maintain linearity within the MILP framework, the tank dynamics are governed by a State of Charge (SOC) formulation, continuously updated by the energy fluxes of the EL (charging) and the FCs (discharging). The physical boundaries of the SOC are constrained by the vessel's minimum and maximum operating pressures, p_{min} and p_{max}, defined from [14] respectively as 3 and 28 Bars. Using in first approach the ideal gas approximation, the minimum and maximum energy capacities ($E_{min,HT}$ and $E_{max,HT}$) of the storage vessel are computed directly from the Lower Heating Value (LHV_{h2}) of hydrogen, as described in Equation 5.

$$E_{min/max,HT} = LHV_{h2} * V_{HT} * \frac{p_{min/max}}{R_{h2} * T} \tag{5}$$

Where V_{HT} is the physical volume of the pressurized vessel, T the constant operating ambient temperature of 20°C, and R_{h2} is the specific gas constant for hydrogen. This establishes the absolute bounds for the discrete-time SOC mass balance equations. The PV system is modelled as an array of commercial modules, utilizing the specifications of a reference panel [18]. The electrical power output is calculated as a function of the incident Global Horizontal Irradiance, the covered area and number of panels and a fixed efficiency. The Thermal Energy Storage (TS) is modelled as a perfectly mixed water tank. Its thermal capacity is derived from the thermodynamic properties of the working fluid, fixing a design temperature difference between the supply and return flows and the tank volume. The electrical batteries are modelled as a modular stack of commercially available units [19], parametrized by number of modules in series and parallel, from which capacity values and maximum charge/discharge rates are determined. A constant charge and discharge efficiency has been imposed. For both the ES and TS, temporal energy shifting is managed via discrete-time state of charge continuity equations. The solver is constrained by maximum and minimum bounds, preventing deep discharge and reflecting the physical degradation limits of the respective technologies. The auxiliary natural gas boiler is integrated into the multi-energy system exclusively as a thermal backup. It acts as a feasibility component for the linear solution, providing an unconstrained thermal energy source andpreventing the solver from reaching an infeasible state during extreme thermal demand.

2.2. Double layer algorithm

To preserve a strictly linear behaviour of the model, the optimization of component sizing was entirely decoupled from the hourly dispatch of energy fluxes. If sizing and dispatch variables were solved simultaneously, constraints governing the power output of scalable components, such as Els and FCs, would require multiplying a variable related to the rated capacity by one related to the operational state. This inevitably introduces bilinear terms, transforming the problem into a Mixed-Integer Nonlinear Programming formulation. While the selected solver can handle specific quadratic constraints, applying them across an 8760-hour horizon would trigger an exponential increase in computational complexity, leading to intractable execution times. To avoid this problem, a bi-level heuristic-deterministic architecture is used. The outer sizing optimization is performed by a genetic algorithmim, each individual in the population represents a distinct configuration of the multi-energy system. The specific genes of each individual define the complete sizing vector: the nominal capacities of the ELs and FCs; the discrete number of PV panels and EB modules; and the physical volumes of the TS and HT. During each generation of the GA, the algorithm passes these candidate sizing vectors to the inner MILP layer as sets of fixed parameters. By stripping the variable sizing out of the internal matrix, the selected solver, Gurobi [20], executes the continuous management problem purely as a Mixed-Integer Linear Program, guaranteeing a globally optimal operational dispatch for that specific hardware configuration. Regarding the objective of the optimization framework, which is to minimize the Net Present Cost (NPC) of the system over its entire operational lifetime (K), while evaluated by the internal solver it serves directly as the fitness score to drive selection, crossover, and mutation of the GA. The NPC aggregates the total Capital Expenditure ($CAPEX$), the discounted annual Operational Expenditures ($OPEX$), the discounted revenues from hydrogen market participation, and a virtual penalty cost representing unmet hydrogen demand. The objective function is

mathematically formulated as the minimization of the total discounted system costs, evaluated as in Equation 6.

$$NPC = CAPEX + \sum_{k=1}^{K} \frac{OPEX_k - Rv_k + \Pi_k}{(1+r)^k} \tag{6}$$

where r is the annual discount rate set at 5%, Rv_k represents the annual revenue generated from selling a predefined fraction of the produced hydrogen to the external market, and Π_k is the financial penalty imposed for unmet hydrogen demand, introduced as a soft constraint to guarantee solver feasibility under all scenarios. The total $CAPEX$ encapsulates the initial investment for all system components, while the annual $OPEX_k$ is defined as the sum of fixed operation and maintenance $(O\&M)$ costs and the time-dependent variable costs associated with grid electricity and natural gas consumption, as described in Equation 7.

$$OPEX_k = O\&M + \sum_{t=1}^{8760} P_{grid,in}(t) * c_{grid}(t) + V_f(t) * c_f(t) \tag{7}$$

where $(O\&M)$ aggregates the capacity-dependent maintenance costs of the active components, defined as a percentage investment cost. $P_{grid,in}(t)$ is the electrical power imported from the grid at the hourly price $c_{grid}(t)$, and $V_f(t)$ is the volumetric fuel consumption of the boiler at the price $c_f(t)$.

2.3. Electrolyser and Fuel Cells degradation

The degradation of Proton Exchange Membrane technologies is an highly documented phenomenon that could fundamentally alters the long-term optimal dispatch of Multi-Energy Systems. To ensure the multi-year simulation accurately reflects real-world ageing, it is necessary to translate physical components degradation into modelled operational efficiency losses. The gradual performance loss in PEM electrolysers and fuel cells is driven by complex, overlapping electrochemical and mechanical stressors. In both technologies, degradation is characterized by membrane thinning, catalyst dissolution, and the corrosion of carbon supports [11]. These degradation modes are significantly accelerated by dynamic, intermittent operation, such as frequent start-stop cycles typical of renewable-coupled microgrids [8]. Rather than applying a percentage penalty to the components, this study models degradation through its voltage drift over operating time. Because the efficiency of PEM technologies is inextricably linked to cell voltage, modelling the voltage variation allows for a direct, dynamic recalculation of the piecewise-linearized efficiency curves. For the Electrolyser, degradation increases internal cell resistance. Consequently, the operating voltage required to maintain a specific current density increases over time, translating directly into higher electrical energy consumption and dropping the efficiency curve. Conversely, for the Fuel Cell, degradation suppresses the output voltage for a given hydrogen consumption rate, resulting in a decrease in the generated electrical power, thereby lowering the electrical efficiency curve. By extracting specific decay rates from the literature and multiplying them by the accumulated operating hours, the model dynamically shifts the nominal efficiency curves downward year over year, forcing the MILP solver to adapt its optimal dispatch to the failing hardware. Establishing a precise voltage decay rate has revealed to be complex, as literature values vary wildly based on specific machine architectures, current densities, and operational testing profiles. For the PEM Electrolyser, [21] report baseline voltage increases of 0.4 to 5 $\mu V/h$, while [10] report drifts of 20 to 50 $\mu V/h$ under highly stressful, high-current ON/OFF scenarios. To maintain a conservative but realistic boundary, this study adopts a degradation rate of 15 $\mu V/h$, aligning with the thresholds reported by [22], while safely discarding the extreme stress-test data that would overpenalize the optimization. For the PEM Fuel Cell, the literature presents even greater variance. Extrapolating the steady-state dataset utilized by [9] yields an unrealistic decay approaching 1.15 mV/h (1150 $\mu V/h$), which was discarded as a three-order-of-magnitude outlier. Furthermore, while [23] report rates of 132 to 169 $\mu V/h$ under constant and intermittent loads, these tests were conducted at current densities over ten times higher than those parametrized in the baseline reference model [14].

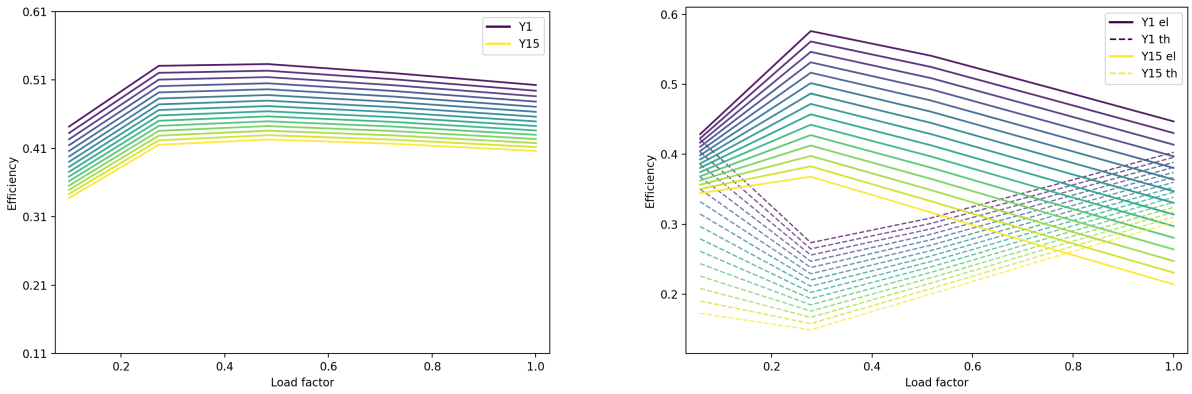

a b

Figure 2: Piecewise linearized efficiency curves of the electrolyser (a) and fuel cell (b) over the simulated years accounting for degradation.

Imposing a 170 $\mu V/h$ penalty on the current MILP architecture prematurely collapses the thermal efficiency to zero, breaking the thermodynamic balance. Consequently, these extreme values were excluded. Instead, the highest value, although obtained for dynamic maritime applications, proposed by [8], was selected, establishing the fuel cell degradation rate at 4.8 $\mu V/h$. To contextualize the impact of the selected degradation rates, Figure 2 illustrates the multi-year evolution of the efficiency curves for both the electrolyser and the fuel cell. For the purpose of this representative projection, the degradation trends are extrapolated manteining the annual operating hours equal to the optimal dispatch profile of the first year. While this static projection provides a clear visual reference of the capacity fade, it must be noted that within the actual sequential MILP simulation, the annual operating hours are not fixed; the solver dynamically re-optimizes the system's yearly dispatch to economically mitigate these exact efficiency losses.

2.4. Case study

The model has been applied in the case of an Italian industrial neighbourhood characterised by the request for electrical and thermal energy, as well as a hydrogen demand. The hourly irradiance data were derived from PVGIS [24] for the city of Padova, while the hourly cost of electricity bought from the grid is based on the Italian national unique price, for the year 2023 [25]. The cost of methane, used to power the boilers, is derived from the GME website [25]. The user loads were modelled starting from literature data [26]. Once the neighbourhood composition was selected to add up to nearly 1000 kWh/day, the monthly mean values were elaborated integrating a randomly generated hourly and daily variation to create more realistic curves. This process has been performed for the electrical and thermal user curve, while the hydrogen curve has been modelled for an internal industrial use. To improve the economic viability of the hydrogen subsystem, an exogenous hydrogen market was integrated into the model. Surplus hydrogen generated by the electrolyser can be exported to this market at a fixed, deterministic price. However, to ensure the optimization algorithm prioritizes the satisfaction of local user energy demands over pure market arbitrage, a strict upper bound of 15% of the nominal capacity was imposed on the export flux. This explicit boundary prevents the sizing the electrolyser exclusively as a commercial hydrogen production facility, constraining external sales and forcing to use the bulk of the hydrogen subsystem for internal power-to-gas-to-power storage cycles. To ensure a comparative analysis, the economic boundary conditions were defined relative to a standard baseline scenario in which the end-user relies solely on a conventional gas boiler and a standard electrical grid connection. Because these elements represent mandatory, pre-existing baseline infrastructure, their installation costs are treated as sunk costs. Consequently, the capital expenditure for the boiler, as well as the one for the grid connection, is explicitly excluded from the objective function. In Table 1 the upper and lower limits of the outer GA optimization variables are reported, in addition

the CAPEX costs of each component.

Table 1: Optimization variables, range and cost for each component of the system

Component	Variable	Range	Cost
PV Plant	N° of panel	0 – 5000 panels	400 €/panel
Electrolyser	Rated Power	0 – 2000 kW	1400 €/kW
Fuel Cell	Rated Power	0 – 1000 kW	2000 €/kW
Hydrogen storage	Volume	0 – 30 m^3	470 €/m^3
Electric battery	N° of modules	0 – 64 modules	300 €/module
Thermal storage	Volume	0 – 500 m^3	400 €/m^3

3. Results

This section details the outcomes of the bi-level optimization and the subsequent multi-year degradation analysis. First, the optimal capacity sizing of the Multi-Energy System is presented. The initial dispatch simulation for the first Year is analysed assuming nominal component efficiencies. Key Performance Indicators (KPIs) are evaluated to comprehensively frame the baseline behaviour. Following the first simulation, the study evaluates the long-term operational impacts of component degradation. By executing sequential, year-over-year dispatch simulations, the operational shifts induced by the progressive efficiency loss in the electrolyser and fuel cell are quantified. Finally, an economic analysis is presented to demonstrate how the physical degradation dynamically alters the operational expenditures and the overall financial feasibility of the MES across the 15-year project horizon.

3.1. Initial optimization

The outer Genetic Algorithm (GA) was parametrized with a population size of 30 individuals and a maximum termination criterion of 30 generations. To ensure computational tractability during the intensive multi-year simulation, the inner MILP model was bounded by dynamic time limits and relative MIP gap thresholds. Table 2 details the optimal capacity sizing vector returned by the GA. The results indicate a substantial deployment of the hydrogen subsystem, with the electrolyser capacity significantly oversized relative to the user demand. This behaviour is a direct algorithmic response to the severe financial penalties imposed within the objective function for unmet loads and the high intermittency of the renewable feed-in. The energy storage components were deployed, with the Battery Energy Storage System capacities sized extremely close to their predefined upper limits. Similarly, also the optimal number of installed PV panels converged near the maximum allowable spatial bound. Economically, the optimization yielded a highly favourable system architecture. The minimized Net Present Cost was evaluated at €26.5 million. When compared to the unoptimized baseline scenario, at a cost of €43.4 million, the bi-level optimization framework achieved a massive lifecycle cost reduction of €16.9 million. A qualitative analysis of the system's operational dynamics is visualized in Figures 3, 4, 5 and 6. It is important to note that the MILP solver evaluates the 8760-hour dispatch utilizing a defined relative MIP gap to ensure computational tractability over the multi-year horizon. Because isolated, single-hour fluctuations carry marginal mathematical weight within the objective function, this analysis strictly evaluates macroscopic dispatch trends rather than granular hourly anomalies. Figures 3 and 4 illustrate the electrical fluxes and the user demand for representative summer, June 21, and winter, January 1, profiles. The dispatch matrix reveals that PV generation overwhelmingly dominates the energy mix. Consequently, the operation of the electrolyser is strictly coupled to solar availability, functioning exclusively during periods of high irradiance to capture the renewable surplus. Conversely, during late afternoon and nocturnal periods, the system relies heavily

Table 2: Variable and Value for each optimized component of the system

Component	Variable	Value
PV Plant	N° of panel	4650
Electrolyser	Rated Power	1000 kW
Fuel Cell	Rated Power	250 kW
Hydrogen storage	Volume	28 m^3
Electric battery	N° of modules	60 modules
Thermal storage	Volume	305 m^3

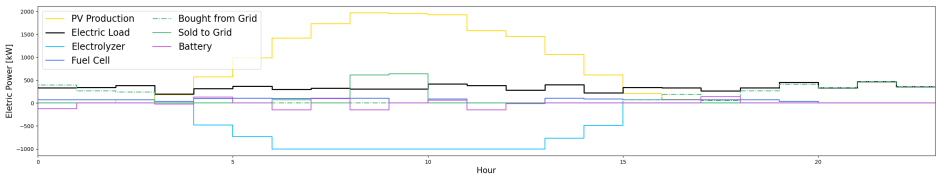

Figure 3: Simulation of the electrical load coverage for a typical day of summer

on external grid imports to satisfy user demand, with the Fuel Cell and Battery Energy Storage System providing marginal contributions. Most notably, during summer, a massive volume of surplus PV generation is exported to the external grid to maintain the energy balance.
In Figures 5 and 6 extend the analysis to the thermal fluxes. The dispatch matrix reveals that the heat produced by the fuel cells and the discharging fluxes of the thermal energy storage equally supply the thermal load. However, despite the presence of the hydrogen subsystem, the traditional auxiliary gas boiler continues to dominate the overall thermal load coverage across both seasons. This operational behaviour frames the hydrogen as a premium, high-cost internal energy carrier, avoiding dispatching the FC solely to satisfy thermal demand. Instead the FC is dispatched primarily as an electrical asset, while heat is captured by the TS to avoid curtailment and smooth out thermal peaks. When the cogenerative heat is insufficient to satisfy the user demand, the solver defaults to the gas boiler.
Finally, Figure 7 illustrates the State of Charge of the pressurized hydrogen storage vessel. The SOC trajectory strictly adheres to the predefined capacity bounds, validating the enforcement of the operational constraints within the formulation. A continuous utilization profile emerges across the entire year, characterized by a highly dynamic charge and discharge cycle. This cycling frequency intensifies significantly during the summer months to absorb the photovoltaic surplus, whereas it dampens during rainy or winter periods. Crucially, the dispatch matrix reveals that the hydrogen tank is utilized primarily as a short-to-medium-term, intra-day to multi-day, energy buffer rather than a long-term seasonal storage mechanism. This behaviour is fundamentally driven by the nature of the exogenous boundary conditions: because the industrial loads maintain a relatively steady demand profile across all seasons, the system does not experience the months-long seasonal energy deficits typically seen in residential applications. Consequently, the solver optimizes the hydrogen stock for rapid, continuous

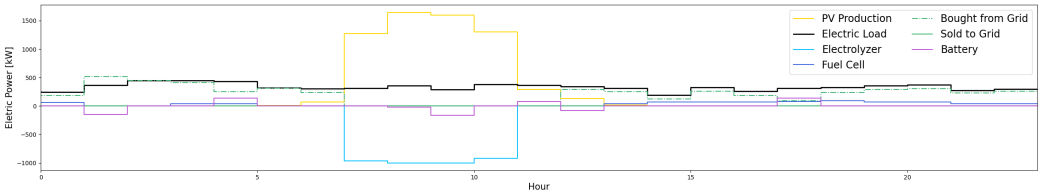

Figure 4: Simulation of the electrical load coverage for a typical day of winter

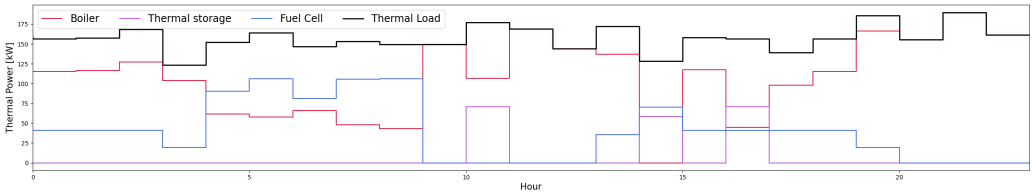

Figure 5: Simulation of the thermal load coverage for a typical day of summer

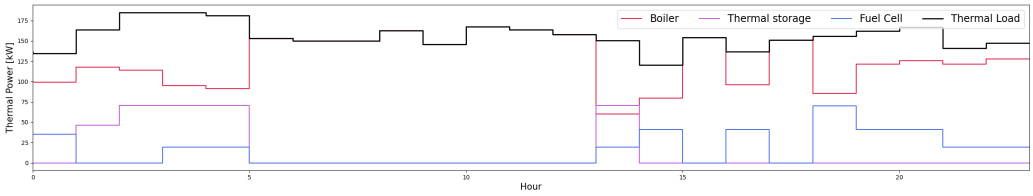

Figure 6: Simulation of the thermal load coverage for a typical day of winter

arbitrage to balance the daily intermittency of the solar array, rather than hoarding it for seasonal shifts. An evaluation of the system's KPIs further quantifies the operational dispatch. The Fuel Cells supply around 8% of the total electrical demand and over 15% of the thermal demand requested by the users, recording relative utilization factors of 31% and 22%, respectively. Concurrently, the oversized electrolyser successfully satisfies 100% of the exogenous hydrogen demand. Despite this complete load coverage, the electrolyser achieves an annual capacity factor of only 21%, reflecting its highly intermittent operation dictated almost entirely by the availability of surplus photovoltaic generation.

3.2. Degradation simulation

To quantify how the gradual capacity fade of the electrolyser and fuel cell impacts the long-term operational dispatch of the system, a sequential multi-year analysis was executed. Following the initial optimization, the accumulated operating hours for each component were extracted at the end of each simulated year. These operational hours were then used to calculate the specific voltage decay and correspondingly downgrade the piecewise-linearized efficiency curves for the subsequent year's simulation. An analysis of the resulting sequential dispatch reveals that despite the steady decline in conversion efficiency, the total number of annual operating hours for both components remains qualitatively constant throughout the 15-year horizon. The system is forced to continue utilizing the degraded hardware because the economic penalties for unmet hydrogen demand—coupled with the high volumetric costs of grid imports and auxiliary boiler gas—remain prohibitively expensive. Because the solver does not drastically curtail the operating hours, the theoretical voltage decay trajectories previously projected in Figure 2 are empirically validated within the dynamic simulation. The macroscopic evolution of the energy fluxes is illustrated in Figure 8, which reports the averaged daily production profiles across the simulated multi-year horizon. While the overarching dispatch architecture remains largely anchored by the rigid system constraints, the internal thermodynamic balance of

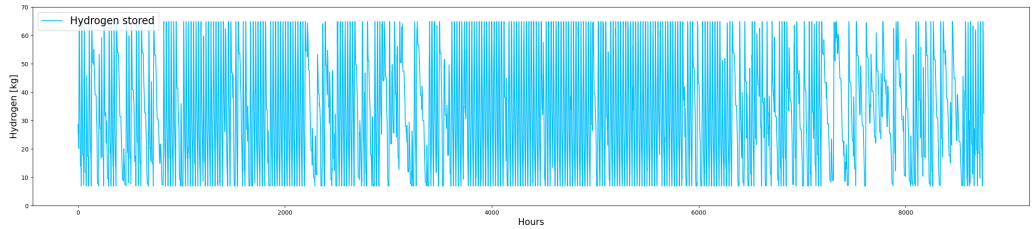

Figure 7: Yearly amount of hydrogen stored in the pressurized hydrogen tank

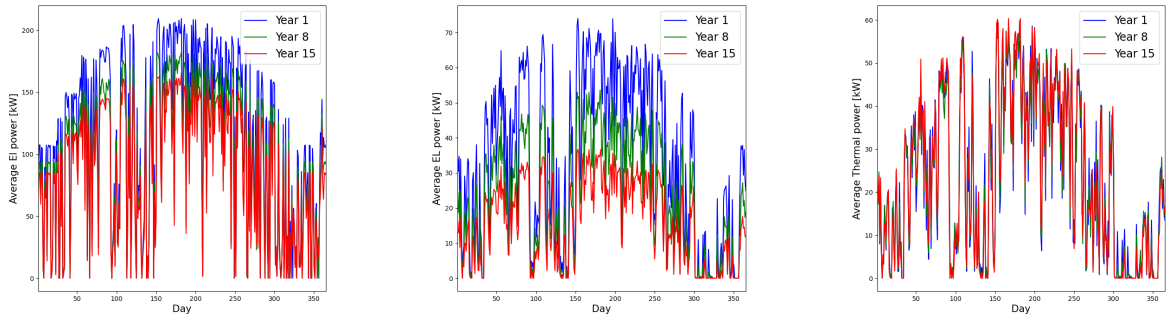

a b c

Figure 8: Average daily energy dispatch profiles over a simulated operational year: (a) Equivalent hydrogen energy produced by the electrolyser; (b) Electrical energy generated by the fuel cell; (c) Recoverable thermal energy output of the fuel cell

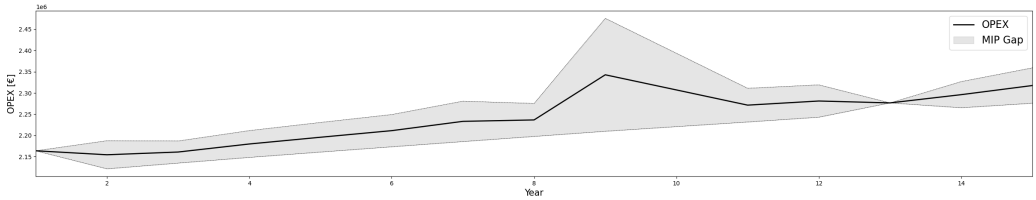

Figure 9: Evolution of the Operational Expenditures across the simulated period associated with the mathematical uncertainty inherent to the solver's relative termination criteria.

the Fuel Cell undergoes a profound shift. As depicted in Figure 8b, the electrical generation of the FC experiences a severe and progressive decline over the years, while the thermal generation remain constant despite the considerable decrease in efficiency.

Finally, evaluating the system dynamics from a techno-economic perspective, Figure 9 illustrates the financial toll of the unmitigated capacity fade. The progressive degradation of the hydrogen subsystem components drives a steady, compounding increase in the annual Operational Expenditures across the simulation horizon. As the internal conversion efficiency drops and the system is forced to procure substitute energy from the traditional sources, the annual OPEX escalates from an initial €2.16 million in Year 1 to €2.31 million by Year 15, representing a 6% total increase in operational costs. While this specific OPEX increase may appear marginal when contextualized against the massive €16.9 million overall NPC savings achieved by the initial optimal sizing, it represents a critical scalability metric. In Multi-Energy Systems characterized by higher capacity factors, where the electrolyser and fuel cell are dispatched more frequently, this efficiency-loss penalty will compound much more aggressively. Consequently, as the global deployment of these renewable technologies accelerates, this analysis proves that the integration of dynamic degradation penalties into techno-economic modelling is absolutely essential to prevent the severe underestimation of long-term operational costs.

4. Conclusions

This study proposed and evaluated a novel, degradation-aware bi-level optimization framework for Hydrogen-Integrated Multi-Energy Systems. By decoupling component capacity sizing, executed via a Genetic Algorithm, from hourly operational dispatch managed by a Mixed-Integer Linear Programming solver, the framework successfully bypassed nonlinear computational bottlenecks while evaluating a 15-year project horizon. Applied to a zero-emission industrial case study, the optimization yielded critical insights for long-term energy planning: Under nominal conditions, the optimal zero-emission architecture prioritized maximized photovoltaic deployment and an aggressively oversized electrolyser (1000 kW) to capture renewable intermittency and avoid unmet load penalties. This

configuration achieved a €16.9 M€ Net Present Cost reduction compared to a fossil-fueled baseline. The sequential multi-year simulation proved that unmitigated capacity fade fundamentally alters optimal system dispatch. Driven by irreversible empirical voltage decay, the electrical generation of the fuel cell severely declines over the system's lifetime, while its thermal output remains constant. Consequently, the fuel cell degrades from a balanced cogeneration asset into a predominantly thermal generator. To compensate for this progressive efficiency loss, the solver is forced to increasingly rely on external grid imports. This dynamic adaptation drives a compunded 6% increase in Operational Expenditures over the 15-year simulation. Ultimately, this research demonstrates that while hydrogen-integrated systems offer profound economic and environmental benefits, assuming static component efficiencies creates blind spots. The integration of dynamic degradation penalties into techno-economic modelling has proved absolutely essential to prevent the severe underestimation of long-term operational costs as the global deployment of these renewable technologies accelerates.

References

[1] International Energy Agency. *World Energy Outlook 2025*. Paris: IEA; 2025 Nov 12. Available at: `https://www.iea.org/reports/world-energy-outlook-2025` [accessed 26.3.2026].

[2] Dalala Z, Al-Omari M, Al-Addous M, Bdour M, Al-Khasawneh Y, Alkasrawi M. Increased renewable energy penetration in national electrical grids constraints and solutions. *Energy* 2022;246:123361. doi:10.1016/j.energy.2022.123361.

[3] Angelico R, Giametta F, Bianchi B, Catalano P. Green Hydrogen for Energy Transition: A Critical Perspective. *Energies* 2025;18(2):404. doi:10.3390/en18020404.

[4] Mekonnin AS, Wacławiak K, Humayun M, Zhang S, Ullah H. Hydrogen Storage Technology, and Its Challenges: A Review. *Catalysts* 2025;15(3):260. doi:10.3390/catal15030260.

[5] Gabrielli P, Flamm B, Eichler A, Gazzani M, Lygeros J, Mazzotti M. Modeling for optimal operation of PEM fuel cells and electrolyzers. In: *2016 IEEE 16th International Conference on Environment and Electrical Engineering (EEEIC)*; 2016 Jun 7-10; Florence, Italy. IEEE; p. 1–7. doi:10.1109/EEEIC.2016.7555707.

[6] Ghany AA, Samy MM. Low pressure PEM electrolyzer system modeling with heat loss representation. *Results in Engineering* 2025;27:105799. doi:10.1016/j.rineng.2025.105799.

[7] Kulikovsky AA, Scharmann H, Wippermann K. Dynamics of fuel cell performance degradation. *Electrochemistry Communications* 2004;6(1):75–82. doi:10.1016/j.elecom.2003.10.018.

[8] McCay K, Karstensen PEE, Gerhardt M, Coolegem J, Damiano D, Lædre S. An analysis of the reversible and irreversible degradation of a PEM fuel cell short-stack operated under simulated maritime conditions. *Journal of Power Sources* 2026;665:239011. doi:10.1016/j.jpowsour.2025.239011.

[9] Chen D, Wu W, Chang K, Li Y, Pei P, Xu X. Performance degradation prediction method of PEM fuel cells using bidirectional long short-term memory neural network based on Bayesian optimization. *Energy* 2023;285:129469. doi:10.1016/j.energy.2023.129469.

[10] Maoulida F, Guilbert D, Camara MB, Dakyo B. Dynamic electrical degradation of PEM electrolyzers under renewable energy Intermittency: Mechanisms, diagnostics, and mitigation strategies – A comprehensive review. *Renewable and Sustainable Energy Reviews* 2026;225:116170. doi:10.1016/j.rser.2025.116170.

[11] Polo-Molina A, Portela J, Rozas LAH, González RC. Modeling Membrane Degradation in PEM Electrolyzers with Physics-Informed Neural Networks. *arXiv* 2025 Jun 19. arXiv:2507.02887. doi:10.48550/arXiv.2507.02887.

[12] Sech E, Benato A, Pecchini M, Peccolo S. A TWO STAGE OPTIMIZATION APPROACH

TO DESIGN AND MANAGING COMPLEX GENERATION SYSTEMS. In: *Proceedings of ECOS 2025: 38th International Conference on Efficiency, Cost, Optimization, Simulation and Environmental Impact of Energy Systems*; 2025 Jun 30–Jul 4; Santorini, Greece. Forthcoming.

[13] Abdin Z, Al Khafaf N, McGrath B, Catchpole K, Gray E. A review of renewable hydrogen hybrid energy systems towards a sustainable energy value chain. *Sustainable Energy Fuels* 2023;7(9):2042–62. doi:10.1039/D3SE00099K.

[14] Marocco P, Ferrero D, Lanzini A, Santarelli M. Optimal design of stand-alone solutions based on RES + hydrogen storage feeding off-grid communities. *Energy Conversion and Management* 2021;238:114147. doi:10.1016/j.enconman.2021.114147.

[15] Buttler A, Spliethoff H. Current status of water electrolysis for energy storage, grid balancing and sector coupling via power-to-gas and power-to-liquids: A review. *Renewable and Sustainable Energy Reviews* 2018;82:2440–54. doi:10.1016/j.rser.2017.09.003.

[16] Li Y, Shang Z, Peng F, Zhao Y, Ren L. Improved control-oriented polarization characteristic modeling for proton exchange membrane water electrolyzer with adaptive hunting game based metaheuristic optimization. *Energy Conversion and Management* 2024;305:118264. doi:10.1016/j.enconman.2024.118264.

[17] Wang Y, Zeng Z, Wang T, Che Z. Dynamic simulation and optimization of a residential proton exchange membrane fuel cell (PEMFC) combined heat and power (CHP) system. *Energy* 2025;319:134865. doi:10.1016/j.energy.2025.134865.

[18] Maxeon Solar Technologies. SunPower Performance 7 Solar Panels [Internet]. Singapore: Maxeon Solar Technologies; 2024 Apr 11. Available at: `https://www.c2ccertified.org/certified-products/maxeon-performance-solar-panels` [accessed 26.3.2026].

[19] BYD Company Limited. *Battery-Box Premium LVS Technical Data Sheet*. Shenzhen, China: BYD Co. Ltd.; 2020 Jun 16. Available at: `https://www.vpsolar.com/download/catalog/Storage/BYD/Premium-LVS/Datasheet_BYD-BBOX-Premium-LVS%20IT.pdf` [accessed 26.3.2026].

[20] Gurobi Optimization, LLC. *Gurobi Optimizer Reference Manual*. Beaverton, OR: Gurobi Optimization, LLC; 2025. Available at: `https://www.gurobi.com` [accessed 26.3.2026].

[21] Yue M, Lambert H, Pahon E, Roche R, Jemei S, Hissel D. Hydrogen energy systems: A critical review of technologies, applications, trends and challenges. *Renewable and Sustainable Energy Reviews* 2021;146:111180. doi:10.1016/j.rser.2021.111180.

[22] Siracusano S, Baglio V, Van Dijk N, Merlo L, Aricò AS. Enhanced performance and durability of low catalyst loading PEM water electrolyser based on a short-side chain perfluorosulfonic ionomer. *Applied Energy* 2017;192:477–89. doi:10.1016/j.apenergy.2016.09.011.

[23] Zuo J, Steiner NY, Li Z, Hissel D. Degradation root cause analysis of PEM fuel cells using distribution of relaxation times. *Applied Energy* 2025;378:124762. doi:10.1016/j.apenergy.2024.124762.

[24] European Commission Joint Research Centre. *Photovoltaic Geographical Information System (PVGIS)* [Internet]. Ispra, Italy: JRC; 2024. Available at: `https://re.jrc.ec.europa.eu/pvg_tools/en/` [accessed 26.3.2026].

[25] Gestore dei Mercati Energetici S.p.A. *GME: Italian Energy Markets Data* [Internet]. Rome, Italy: GME; 2026. Available at: `https://www.mercatoelettrico.org/` [accessed 26.3.2026].

[26] Macchi E, Campanari S, Silva P. *La microcogenerazione a gas naturale*. Milan, Italy: Polipress; 2005. ISBN: 9788873980162.